IEEE Access
Multidisciplinary | Rapid Review | Open Access Journal

Received 11 December 2022, accepted 20 December 2022, date of publication 22 December 2022,
date of current version 29 December 2022.

Digital Object Identifier 10.1109/ACCESS.2022.3231751

RESEARCH ARTICLE

MPC-Based Virtual Energy Storage System Using PV and Air Conditioner to Emulate Virtual Inertia and Frequency Regulation of the Low-Inertia Microgrid

JONGLAK PAHASA[1], (Member, IEEE), POTEJANASAK POTEJANA[2], AND ISSARACHAI NGAMROO[3], (Senior Member, IEEE)

[1]Department of Electrical Engineering, School of Engineering, University of Phayao, Phayao 56000, Thailand
[2]Department of Industrial Engineering, School of Engineering, University of Phayao, Phayao 56000, Thailand
[3]Department of Electrical Engineering, School of Engineering, King Mongkut's Institute of Technology Ladkrabang, Bangkok 10520, Thailand

Corresponding author: Jonglak Pahasa (jonglak.pa@up.ac.th)

This work was supported by the National Research Council of Thailand.

ABSTRACT Grid-connected large-scale power converter-based intermittent renewable energy sources (RES) reduce system inertia, increase frequency fluctuation, and increase the rate of change of frequency (RoCoF). An energy storage system (ESS) is an indispensable component of a smart grid, and is used to overcome low-inertia problems. However, the capital and maintenance costs of ESS are high and high RoCoF events are less frequent in power systems. Therefore, the introduction of a virtual energy storage system (VESS) to provide the function of a conventional ESS for power system ancillary services is an innovative and cost-effective method. This study investigated a VESS using photovoltaic (PV) generators and inverter air conditioners (IACs) to provide virtual inertia and frequency regulation for a low-inertia microgrid. A model predictive control (MPC)-based VESS regulates indoor temperature, microgrid frequency, and RoCoF. The impact of parameter variation, that is, the microgrid frequency weight, indoor temperature weight, virtual inertia gain, and number of IACs, was studied and selected by considering the ability of the parameters to provide virtual inertia and frequency regulation. Finally, the efficiency and robustness of the proposed MPC-based VESS technique are compared with those of a conventional VESS. Simulation results revealed that the proposed MPC-based VESS can improve the virtual inertia, reduce the frequency deviation, and reduce the RoCoF of the studied microgrid. In addition, the proposed method is robust to variations in the system parameters.

INDEX TERMS Virtual energy storage system, virtual inertia emulator, load frequency control, inverter air conditioner, photovoltaics generator, microgrid.

I. INTRODUCTION

The recent trend toward environmentally friendly power systems has resulted in an extreme increase in the installation of renewable energy sources (RES). Generally, an RES is connected to the main grid via a power electronic converter [1], [2], [3], [4]. Thus, grid-connected large-scale power electronic converter interfaces with intermittent RES reduce the system inertia, increase the frequency fluctuation, and increase the rate of change of frequency (RoCoF) in the event of contingencies [1], [2], [3], [4]. A higher RoCoF has a major impact on power systems, that is, it (1) increases the wear and tear in generators and reduces the generators' commercial life, (2) causes catastrophic failure of the generating unit, and (3) leads to cascaded tripping, load shedding, and eventually a blackout [4]. Blackouts caused by RoCoFs were studied in [5] and [6].

Energy storage systems (ESS) can be employed to provide virtual inertia emulators and frequency regulation [1], [2], [3], [4]. Nevertheless, the capital and maintenance costs of ESS

The associate editor coordinating the review of this manuscript and approving it for publication was Wanqing Zhao.

are high and high RoCoF events are less frequent in power systems [4]. Therefore, employing an ESS only for virtual inertia emulators is not economically feasible [1], [4].

Recently, virtual energy storage systems (VESS) for power system ancillary services have been proposed by several researchers [7], [8], [9], [10], [11], [12]. A VESS is a cost-effective method for emulating the functions of a conventional ESS [7], [8], [9]. A VESS can adjust its generation output or load to satisfy power system requirements for ancillary services. Ding et al. [9] proposed a VESS for multi-period economic dispatch. A VESS applied to the energy management of an optimally sized DC grid is presented in [10]. In [11], the VESS was used to maximize wind profit by considering the behavior of electricity customers. Vijayalakshmi et al. [12] predicted the VESS capacity of an air-conditioner. This study demonstrated that the VESS capacity depends on the gap between the setpoint and the ambient temperature. A study in [7] showed that a VESS can provide low-, high-, and continuous-frequency responses in a manner similar to a conventional ESS. The concept of a VESS from building loads to provide frequency regulation services was also presented in [8].

Smart loads can be utilized as a VESS, as presented in [12]. In addition, smart loads can be used in virtual inertia emulators and frequency regulation [13], [14], [15]. Smart loads, such as noncritical motors [14], [15] and inverter air conditioners (IACs) [16], [17], [18], [19], [20], [21] can be applied for frequency regulation. The contribution of smart loads to the rapid frequency response of the Great Britain transmission system was studied in [13]. Inverter air conditioners applied to frequency regulation were proposed in [17]. Owing to the heat preservation properties and short-term regulation of the operating power of inverter air conditioners for frequency regulation, the operating power of the inverter air conditioners has little effect on room temperature control [17]. Nevertheless, the application of IACs to provide virtual inertia has not been studied in the literature. Owing to the inverter-interfaced power system of IACs, they can be used to emulate virtual inertia and frequency regulation. However, the application of IACs to emulate virtual inertia should consider their ability to consume/release power during contingencies. As reported in [12], the virtual energy storage capacity of an air conditioner depends on its set-point and ambient temperature. On hot days, inverter air conditioners consume high power to lower the high temperature to the setpoint. Thus, the IACs may hit the maximum power limit and may not consume more power to emulate virtual inertia. Therefore, a method that combines IACs with other devices to emulate the virtual inertia on hot days is required.

In addition, distributed RES, such as photovoltaic (PV) and wind turbine generators, have been applied to provide virtual inertia and frequency regulation. For PV and wind turbine generators, deloading and inertia emulation are the two primary techniques used to provide virtual inertia and frequency regulation [22], [23], [24], [25], [26], [27], [28]. The deloading of the PV generation may not be economically reasonable when the load demand is high. In addition, for a higher economic aspect, the PV systems should be operated at maximum power point tracking (MPPT) and generation should be reduced to provide virtual inertia and frequency regulation. A reduction in the PV generation to provide over-frequency regulation may not solve the under-frequency problem. In addition, PV generation cannot support virtual inertia during the nighttime. Therefore, a method that combines the PV power generation with other devices that can operate daily is required.

As explained above, the PV generator produces power in the daytime and can emulate virtual inertia and frequency regulation during the daytime. In addition, the IAC can emulate virtual inertia and frequency regulation throughout the day but is not able to consume more power during the daytime because of high temperatures, and the IAC may work at the maximum power limit. Therefore, the VESS from the PV generator and IAC is a promising combination of generation and load used to support virtual inertia and frequency regulation. A VESS using a PV generator and IAC was investigated in this study.

On the other side, model predictive control (MPC) is an adaptive control algorithm in which a plant's dynamic model is used to predict the control signal while optimizing the plant output. MPC has been widely accepted in many practical fields [19], [20], [29], [30], [31], [32]. As reported in the literature, MPC has been applied to virtual inertia and frequency regulation with promising results [19], [20], [29], [30]. The MPC applied for controlling inverter air conditioners was proposed in [19] and [20]. In [19], the MPC of the inverter-air conditioning load control was used to regulate the frequency of the power system with communication delay. The simulation results imply that MPC is robust to communication delays when compared with a proportional integral (PI) controller. An MPC-based inverter air conditioner control to regulate indoor temperatures and the frequency deviation of the microgrid was proposed in [20]. The simulation results implied that MPC had a performance effect on the PI controller.

In this study, an MPC-based VESS is investigated to provide virtual inertia and frequency regulation. The VESS controller consists of two loops: an MPC-based frequency and indoor temperature control loop and an MPC-based virtual inertia control loop. The proposed VESS comprises of PV generators and IACs. The main contributions of this study has 3 subjects as follows:

(1) We propose new VESS control techniques for virtual inertia and frequency regulation using MPC. The proposed VESS comprises PV generators, and the IACs can provide virtual inertia and frequency regulation for an entire day without a battery energy storage system. The main VESS component was the IACs, whereas the auxiliary VESS component was the PV generator. Considering the charging/discharge capacity of the IACs load and PV generator, the proposed VESS can support virtual inertia and frequency regulation for an entire day without an energy storage system.

(2) We propose a new control technique that uses two MPCs to control indoor temperature, microgrid frequency, and virtual inertia. Two MPCs were used to control the VESS output power with different control objectives. The first MPC controls the indoor temperature and regulates the microgrid frequency. The second MPC controls the virtual inertia emulators.

(3) The proposed method can use nearly the maximum power of PV generation, that is, the non-reserve power of the PV generators for the virtual inertia emulator. Under normal operating conditions, PV generators operate at maximum power point tracking (MPPT). When the excess power from the IACs is insufficient to provide virtual inertia, the PV generators reduce power generation to support the virtual inertia emulators. Thus, the total surplus power used to provide virtual inertia of the non-reserve PV power is lower than that of the reserve PV power.

The remainder of this paper is organized as follows. Section II describes the study system and its model. The concept of a virtual energy storage system is introduced in Section III. Section IV explains the proposed MPC-based virtual energy storage system using PV generators and IACs to provide virtual inertia and frequency regulation. In Section V, the proposed virtual energy storage system is validated by simulation on a low-inertia microgrid. Finally, Section VI concludes the paper.

II. STUDY SYSTEM AND MODELLING

A. MICROGRID

Figure 1 shows the microgrid used in this study. The microgrid consists of a 30 MW diesel generator, 7.5 MW wind power generator, 8.5 MW PV generator, 20 MW inverter air conditioner load, and 8 MW conventional load (except inverter air conditioners) [20], [29]. None of the power generators are equipped with an inertia or damping controller. Hence, wind and PV power generation drastically changes the microgrid operating point and reduces the system inertia and damping properties. Thus, the stability and performance of the microgrid are reduced. To overcome this problem, a virtual energy storage system (VESS) using PV power generation and inverter air conditioners is applied to provide virtual inertia and frequency regulation service of the microgrid.

B. FREQUENCY RESPONSE OF THE MICROGRID

Figure 2 shows the linearized model of the studied microgrid with the proposed MPC-based VESS for virtual inertia and frequency regulation. Considering the roles of inertia (H), damping (D), and the difference between supply and demand, the frequency deviation (Δf) can be obtained as:

$$\Delta f = \frac{1}{2H\,s + D}\left(\underbrace{\Delta P_{DS} + \Delta P_{PV} + \Delta P_{WTG}}_{\text{generated power}}\right.$$

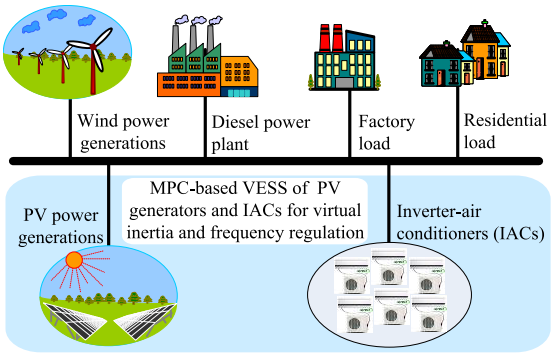

FIGURE 1. Microgrid with VESS of PV generators and IACs for virtual inertia and frequency regulation.

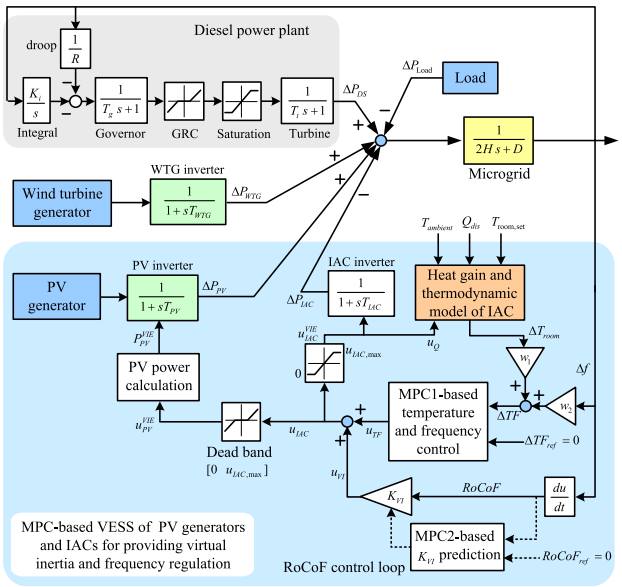

FIGURE 2. A linearized model of the studied microgrid with the proposed MPC-based VESS.

$$\left.\underbrace{-\Delta P_{Load} - \Delta P_{IAC}}_{\text{demanded power}}\right) \quad (1)$$

The net power generated is the cumulative effort of the diesel generator (ΔP_{DS}), PV generator (ΔP_{PV}), and wind turbine generator (ΔP_{WTG}) power systems to counter the active conventional load demand (ΔP_{Load}) and IAC demand (ΔP_{IAC}). Therefore, the microgrid with cumulative inertia H and damping coefficient D slows down RoCoF.

The RoCoF response of the microgrid can be defined as [27],

$$RoCoF = (Hz/s) = \frac{df}{dt} = \frac{f(t) - f(t_{pre})}{t - t_{pre}}, \quad t > t_{pre} \quad (2)$$

where t and t_{pre} are the current and the latest output simulation times respectively, $f(t)$ the frequency at time t, and $f(t_{pre})$ the frequency at time t_{pre}.

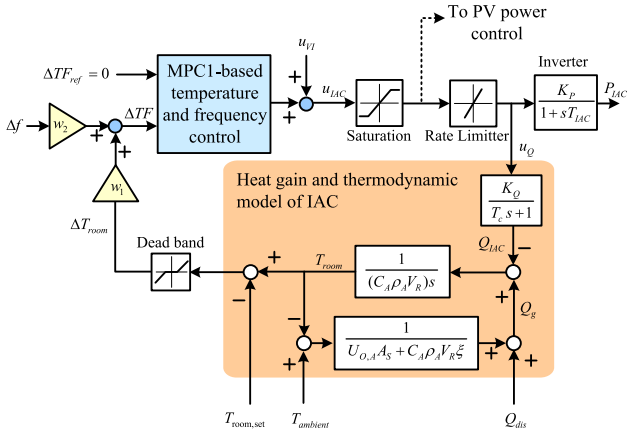

FIGURE 3. A linearized model of the IACs for frequency regulation support.

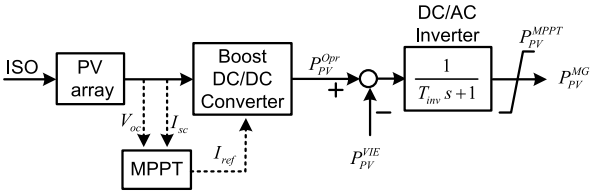

FIGURE 4. Simplify linearized model of PV generator connected to microgrid for virtual inertia emulation.

C. INVERTER AIR CONDITIONER MODEL FOR VIRTUAL INERTIA AND FREQUENCY REGULATION SERVICE

The linearized model of the inverter air conditioner shown in Fig. 3 is composed of a heat gain and thermodynamic model of the room, and an electrical model.

1) The heat gain and thermodynamic model of the room are shown at the bottom of Fig. 3. The thermal model of the room represents the relationship between the room (indoor) temperature and the room's thermal deviation from the refrigeration capacity of the air conditioner. The indoor temperature (T_{indoor}) regulated by IACs is defined as follows:

$$T_{indoor} = \frac{Q_g - Q_{IAC}}{C_A\,\rho_A\,V_R\,s} \tag{3}$$

where Q_{IAC} is the refrigeration capacity of the inverter air conditioner, C_A is the heat capacity, ρ_A is the density of the air, and V_R is the room volume. Q_g is the total heat gain of the room that comes from the heat transfer between the indoor and outdoor air and can be defined as

$$Q_g = (U_{O,A}S_R + C_A\,\rho_A\,V_R\xi)(T_{ambient} - T_{indoor}) + Q_{dis} \tag{4}$$

where $U_{O,A}$ denotes the heat-transformation coefficient, ξ denotes the air-exchange coefficient, and S_R denotes the room surface. $T_{ambient}$ is the ambient temperature and Q_{dis} is the heat radiation from disturbances such as lights, appliances, and people.

2) The electrical model of the inverter air conditioner represents the inverter-interface air conditioner. By adjusting the operating frequency, the compressor of the air conditioner could continuously change its speed. The refrigeration capacity and operating power of the air conditioner were regulated by the operating frequency. The operating power deviation (ΔP_{IAC}) and refrigerating capacity deviation (ΔQ_{IAC}) of the air conditioner can be expressed as:

$$\Delta P_{IAC} = \frac{K_P}{T_{IAC}s + 1}\Delta f_{IAC} + \mu_P \tag{5}$$

$$\Delta Q_{IAC} = \frac{K_Q}{T_c s + 1}\Delta f_{IAC} + \mu_Q \tag{6}$$

where Δf_{IAC} is the operational frequency deviation of the air conditioner, T_{IAC} is the time constant of the inverter, and T_c is the compressor time constant. K_P, K_Q, μ_P, and μ_Q are the constant coefficients.

The relationship between the operating power of the inverter air conditioner (P_{IAC}) and the refrigeration capacity of the IACs (Q_{IAC}) can be expressed as

$$Q_{IAC} = \frac{K_Q}{K_P}P_{IAC} + \frac{K_P\mu_Q - K_Q\mu_P}{K_P} \tag{7}$$

The frequency deviation of the inverter air conditioner (Δf_{IAC}) mostly depends on the difference between the set-point and present indoor temperatures. The Δf_{IAC} can be expressed as

$$\Delta f_{IAC} = K_1\,\Delta T_{indoor} \tag{8}$$

where K_1 is the temperature controller and ΔT_{indoor} is the indoor temperature deviation.

If an inverter air conditioner is used for microgrid frequency control, the operating frequency of the inverter air conditioner should be manipulated by the microgrid frequency. The Δf_{IAC} can be defined as

$$\Delta f_{IAC} = K_1\,\Delta\,T_{indoor} + K_2\,\Delta f \tag{9}$$

where K_2 is the microgrid frequency controller provided by the inverter air conditioner ancillary service.

D. PHOTOVOTAIC MODEL FOR VIRTUAL INERTIA AND FREQUENCY REGULATION SERVICE

Figure 4 shows the simplified linearized model of the PV generator connected to the microgrid for virtual inertia and frequency regulation service. The maximum power point tracking (MPPT) controller is based on perturb and observe algorithms [29].

1) NORMAL OPERATING CONDITIONS

PV generators do not support virtual inertial emulators. The PV power generation used to support virtual inertia is zero, that is, $P_{PV}^{VIE} = 0$. An MPPT controller equipped with a boost DC/DC converter is used to track the maximumPV output power. Consequently, boost DC/DC converter outputpower is supplied to the DC/AC inverter at the maximum power point. The relationship between the PV power generation feed to the microgrid (P_{PV}^{MG}) and the PV operating power (P_{PV}^{Opr}) can be expressed as:

$$P_{PV}^{MG} = P_{PV}^{Opr} - P_{PV}^{LOSS}, \tag{10}$$

where P_{PV}^{LOSS} is the power loss of the PV inverter.

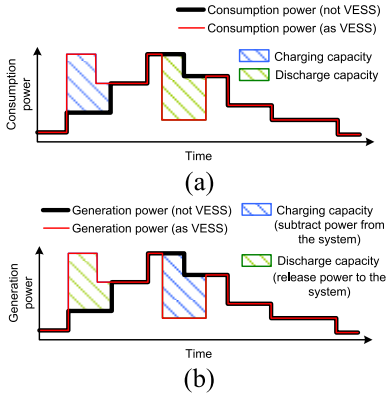

FIGURE 5. Virtual energy storage system capacity (a) controllable load (b) controllable source.

2) PV GENERATORS USED FOR VIRTUAL INERTIA EMULATORS

In this case, the PV generator reduces the power generation for the virtual inertia emulator, that is, $P_{PV}^{VIE} \neq 0$. The PV power feed to the microgrid is the operating PV generation subtracted by the power of the virtual inertia emulators and power loss. The PV power generation supply to the microgrid can is expressed as in (11).

$$P_{PV}^{MG} = P_{PV}^{Opr} - P_{PV}^{VIE} - P_{PV}^{LOSS}. \tag{11}$$

III. VIRTUAL ENERGY STORAGE SYSTEM

A. CONCEPT OF VIRTUAL ENERGY STORAGE SYSTEM

Virtual energy storage systems (VESS), like a virtual power plant (VPP) systems, combine various controllable electrical components, such as ESSs, flexible loads, and distributed generators [8], [12], [33]. The VESS aims to store surplus or release electric power according to system needs. The VESS can be integrated with the power network operation and its energy exchange can vary with the power grid owing to the external control signal. The difference between the VPP and VESS is a major role in the power system. The VPP is considered as a generator that releases power to the system, whereas the VESS is regarded as the energy storage system. The VESS charge/discharge power to/from the power system.

B. CAPACITY OF VIRTUAL ENERGY STORAGE SYSTEM

The virtual energy storage considered here is a controllable load and controllable generation. The virtual energy storage capacity of the controllable load is shown in Fig. 5 (a) [8]. When the virtual energy storage of the load consumes more power than the conventional load, the surplus power is the charging capacity. When the virtual energy storage of the load consumes less power than the conventional load, the release power is the discharge capacity.

Figure 5 (b) shows the virtual energy storage capacity of the controllable source (generator). When the virtual energy storage of the generator produces more power than a conventional generator (not virtual energy storage), the surplus power is the discharge capacity. When the virtual energy storage of the generator produces less power than that of the conventional generator, the released power is the charging capacity.

IV. PROPOSED MPC-BASED VIRTUAL ENERGY STORAGE SYSTEM USING PV AND IAC FOR VIRTUAL INERTIA AND FREQUENCY REGULATION

A. VIRTUAL ENERGY STORAGE SYSTEM USING IAC AND PV CAPACITY

Based on [8], the total possible virtual energy storage of IACs can be displayed as shown in Fig. 6 (a). The IACs can be used as virtual energy storage all day. However, during the daytime (8.00-18.00 h), the ambient temperature was very high. The VESS charging capacity may not be sufficient to support virtual inertia and frequency regulation, because of the high IAC power used to regulate the difference between the setting and ambient temperatures.

PV and wind turbine generators can be used to reduce system inertia, as proposed in the literature [22], [23], [24], [25], [26], [27], [28]. Nevertheless, the main contribution of this study is the use of inverter air conditioners as the main component of virtual energy storage systems to provide virtual inertia and frequency regulation. Owing to the high ambient temperature during the daytime, the IAC may operate at the maximum power consumption and may not provide sufficient power to support the virtual inertia emulator. Wind turbine generators can be used as part of the virtual energy storage system in this study. However, conventionally, the wind speed during the day was lower than that at night [37]. Wind power generation during the daytime may not be sufficient for frequency regulation in this study. Therefore, the PV generator is used in this work because PV generators operates in the daytime and can reduce power to support frequency regulation when the IACs cannot consume more power to regulate the microgrid frequency.

Figure 6 (b) shows the total possible VESS capacity of the PV generator. The PV generators can support virtual inertia emulators and frequency regulation during the day. However, when the PV generator operates at the maximum power generation, the charging capacity VESS (reduce power generation) is performed.

Figure 6 (c) shows the total VESS capacities of the IACs and PV generators. VESS capacity was sufficient to support the virtual inertial emulator throughout the day.

B. VIRTUAL ENERGY STORAGE SYSTEM FOR INERTIA AND FREQUENCY REGULATION SERVICE

The virtual energy storage of the PV generators and IACs for virtual inertia and frequency regulation is shown in Fig. 7 [22], [23], where K_{VESS}^{VI} and K_{VESS}^{D} are the virtual inertia gain and damping gain of the VESS, respectively, ΔP_{VESS}^{VIE} is the VESS power consumption deviation for VIE, ΔP_{VESS}^{Opr} is the VESS operating power deviation, and ΔP_{VESS}^{MG} is the deviation of the VESS power to the microgrid. $\Delta P_{VESS}^{\min}$ and

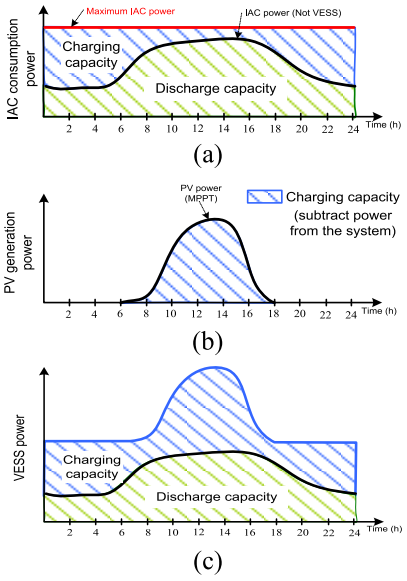

FIGURE 6. Total VESS capacity (a) IACs (b) PV generators (c) IACs and PV generators.

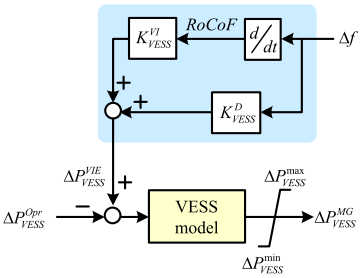

FIGURE 7. The VESS for virtual inertia and frequency regulation service.

$\Delta P_{VESS}^{\max}$ are the minimum and maximum limits of VESS power deviation, respectively.

C. MPC-BASED VESS FOR VIRTUAL INERTIA AND FREQUENCY REGULATION

The proposed MPC-based VESS for virtual inertia and frequency regulation is shown at the bottom of Fig. 2. The VESS controller consists of two loops: (1) the MPC1-based indoor temperature and microgrid frequency regulation control loop and (2) the MPC2-based virtual inertia (or RoCoF) control loop.

In the first loop, the MPC1 simultaneously regulates the indoor temperature to a reference value and reduces the power system frequency deviation. The inputs of MPC1 consisted of indoor temperature and frequency deviations, which were appropriately weighted. The objective of the weighting was to control the indoor temperature and reduce the frequency deviations to within the acceptable ranges. In the second loop, MPC2 predicts the inertial gain of the virtual inertia emulator. The predicted inertial gain is used to produce the RoCoF control signal. Thus, MPC2 regulates RoCoF deviation ($\Delta RoCoC$) to the reference value ($\Delta RoCoC_{ref}$). Finally,

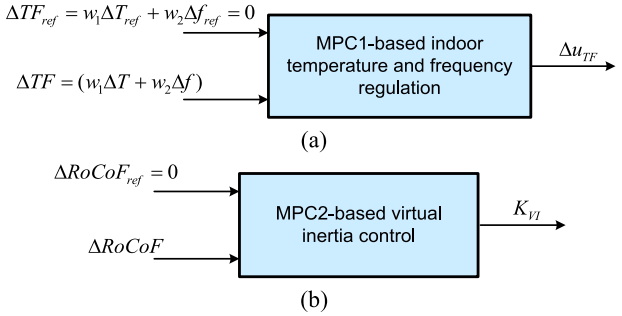

FIGURE 8. Concept of MPC-based VESS control (a) MPC1 (b) MPC2.

the control signals from the MPC1 and MPC2 loops were summed to obtain the control signal for regulating VESS power.

Furthermore, during the day, IAC power consumption may reach its maximum limit. Thus, IACs may not consume more power to reduce high RoCoF and frequency deviation during contingencies. The regulation of PV power generation from maximum power point tracking is used to help IACs support the virtual inertia emulator, as shown in Fig. 6(c).

When IACs are used for frequency regulation, as shown in (9), they can regulate the indoor temperature and power system frequency by tuning the parameters K_1 and K_2, which can be replaced by controllers such as proportional-integral (PI) and MPC controllers. However, in [14] the authors demonstrate that the MPC controller has the performance effects of regulating the indoor temperature and frequency deviations over the PI controller. Therefore, in this study, MPC controllers controlled the power consumption of the IAC to regulate indoor temperature and frequency deviations.

MPC1-based indoor temperature and frequency controls are shown in Fig. 8 (a). The feedback control signal (Δu_{TF}), calculated using MPC1, was employed to control indoor temperature and frequency deviation. The input of MPC1 was the summation of the weighted indoor temperature deviation ($w_1 \Delta T$) and the weighted frequency deviation ($w_2 \Delta f$). The selection of indoor temperature weight w_1 and frequency weight w_2 is important because temperature deviation (ΔT) and frequency deviation (Δf) are affected by indoor temperature weight w_1 and frequency weight w_2, respectively. Figure 8 (b) shows MPC2-based virtual inertia control. The inputs and outputs of MPC2 are the rate of change of the frequency deviation ($\Delta RoCoF$) and initial gain of the VESS (K_{VI}), respectively.

Figure 9 shows the impact of MPC1's input weights (w_1 and w_2) on the absolute indoor temperature deviation $|\Delta T_{indoor}|$ and absolute frequency deviation $|\Delta f|$. This figure is related to Equations (8) and (9). For explanatory purposes, this section uses w_1 and w_2 instead of K_1 and K_2, respectively. In addition, ΔT_{indoor} and Δf in Equations (8) and (9) are changed to $|\Delta T_{indoor}|$ and $|\Delta f|$, respectively. Therefore, Equation (9) can be rewritten as:

$$\Delta f_{IAC} = w_1 \ |\Delta T_{indoor}| + w_2 \ |\Delta f| \tag{12}$$

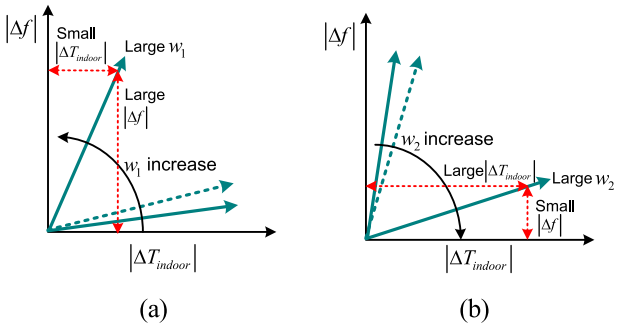

FIGURE 9. Impact of MPC1's input weights to $|\Delta f|$ and $|\Delta T|$ (a) impact of w_1 (b) impact of w_2.

As shown in Fig. 8 (b), when w_1 increases (w_2 = constant), $w_1\Delta T$ increases and is minimized by the MPC1 procedure (see Fig. 8 (a)). Therefore, the indoor temperature deviation ΔT reduced more than the frequency deviation Δf. The red dotted lines indicate that a large indoor temperature weight w_1 produces a small indoor temperature deviation ΔT, and a large frequency deviation Δf. As shown in Fig. 8 (c), when the frequency weight w_2 increases (w_1 = constant), $w_2\Delta f$ increases and is minimized by the MPC1 procedure (see Fig. 8 (a)). Therefore, the frequency deviation Δf reduced more than the indoor temperature deviation ΔT. The red dotted lines indicate that a large frequency weight w_2 produces a small frequency deviation Δf, and a large indoor temperature deviation ΔT. For simplicity, the signs ($\pm$) of the indoor temperature deviation ΔT and microgrid frequency deviation Δf are not considered. The signs of the indoor temperature and frequency deviations are shown in the subsection on tuning temperature and frequency weights.

V. SIMULATION RESULTS AND DISCUSSION

MATLAB/Simulink programming was used to evaluate the effectiveness of the proposed MPC-based VESS for PV generators and IACs in mitigating virtual inertia and regulating microgrid frequency deviation. MPC was performed using the MPC toolbox of MATLAB/Simulink [30]. A microgrid, as shown in Figs. 4-5, was used as the study system. Table 1 lists the parameters [17], [29].

Figure 10 shows the random wind power, solar insolation, and load demand for Cases 1-3. In Case 1, a wind power generation 0.1 pu. disconnected from the microgrid at 200 s, and reconnected at 500 s. In this case, solar insolation oscillates between 700 and 900 w/m^2. The load demand is oscillated around 0.7 pu. For Cases 2-3, the wind power generation 0.1 pu. connected to the microgrid at 100, 400, and 700 s. The solar insolations in Case 2 oscillated in the opposite directions to those in Case 1. In these cases, the load demand oscillate between 0.68 pu. to 0.71 pu. which is higher than that in Case 1.

A. IMPACT OF MICROGRID FREQUENCY WEIGHT

The impact of the microgrid frequency weight (w_2) on RoCoF, frequency deviation, indoor temperature, and IAC power during w_1 = 1 is shown in Fig. 11. The increase in frequency weight w_2 reduces the RoCoF and frequency deviation, and increases the indoor temperature deviation and IAC power. The simulation results imply that increasing the frequency weight w_2 improves frequency stabilization and inertia emulation. The relationship between the frequency and indoor temperature deviations (bottom of Fig. 11) demonstrates that increasing the frequency weight w_2 reduced the frequency deviation and increased the indoor temperature deviation. These simulation results were consistent with those shown in Fig. 8 (c). Considering the ability of w_2 to regulate RoCoF, regulate microgrid frequency, and provide the

TABLE 1. System parameters.

Parameters	Values
Reference frequency, f_{ref} (Hz)	50
Inertia constant, H (sec)	0.06
Damping characteristic of load, D (pu)	0.12
Governor time constant, T_g (sec)	0.1
Turbine time constant, T_t (sec)	0.4
Primary droop factor, R (Hz/pu.MW)	2.4
Secondary frequency controller, K_i (sec)	0.2
Total number of IAC (units)	4000
Capacity of IAC (kW)	4
Time constant of the compressor of the IAC, T_c (sec)	0.02
Compressor of the IAC gain, K_P (kW/Hz)	0.04
Feedback heat gain of the IAC, K_Q (kW/Hz)	0.12
Heat capacity of the air, C_A (kJ/kg.°C)	1.005
Density of the air, ρ_A (g/m^3)	1.205
Air exchange times, ξ (1/h)	0.50
Heat transfer coefficient, $U_{O,A}$ (W/m^2.°C)	3.60
Heat power of disturbances, Q_{dis} (kW)	0.43

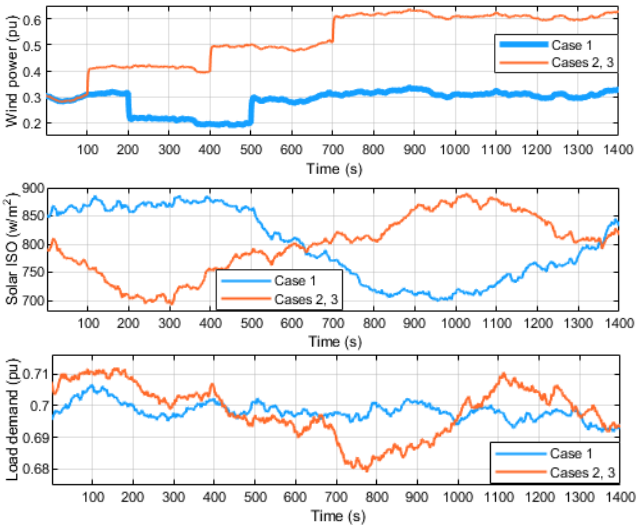

FIGURE 10. Random wind power, solar insolation, and load demand (except IAC).

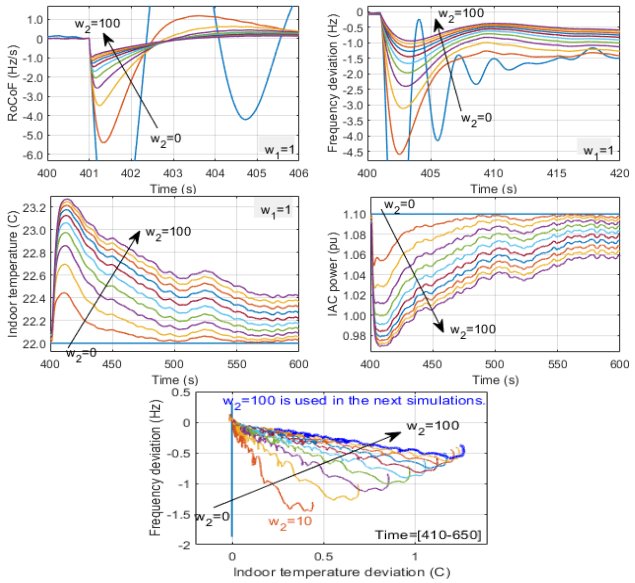

FIGURE 11. Simulation results: w_2 changes, $w_1 = 1$.

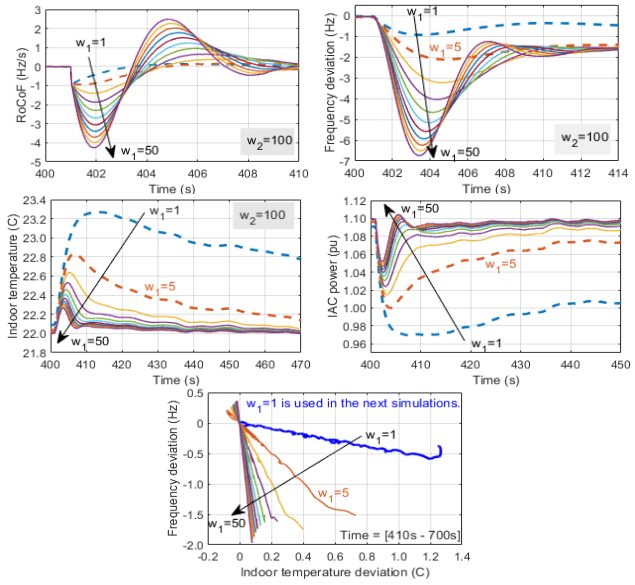

FIGURE 12. Simulation results: w_1 changes, $w_2 = 100$.

maximum indoor temperature within the acceptable range of ($\Delta T_{indoor} < 1.5\,^{\circ}C$), the frequency weight $w_2 = 100$ was selected as the appropriate microgrid frequency weight. Subsequently, the temperature weight w_1 varies, and is selected as the best one in the next subsection.

B. IMPACT OF INDOOR TEMPERATURE WEIGHT

The impact of the indoor temperature weight (w_1) on RoCoF, frequency deviation, indoor temperature, and IAC power during $w_2 = 100$ is shown in Fig. 12. Increasing the indoor temperature weight w_1 can improve the indoor temperature regulations but increases the RoCoF and frequency deviations. The relationship between the frequency deviation and indoor

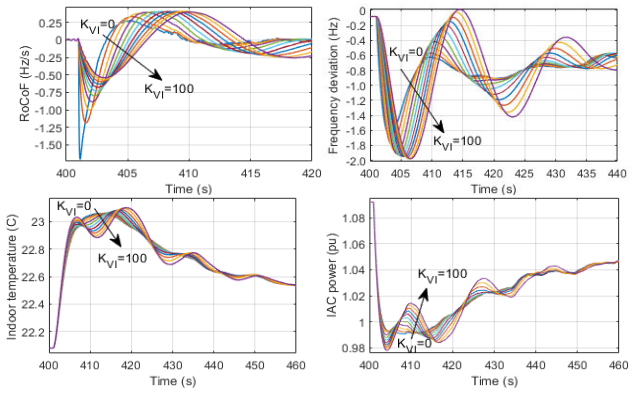

FIGURE 13. Simulation results: K_{VI} changes.

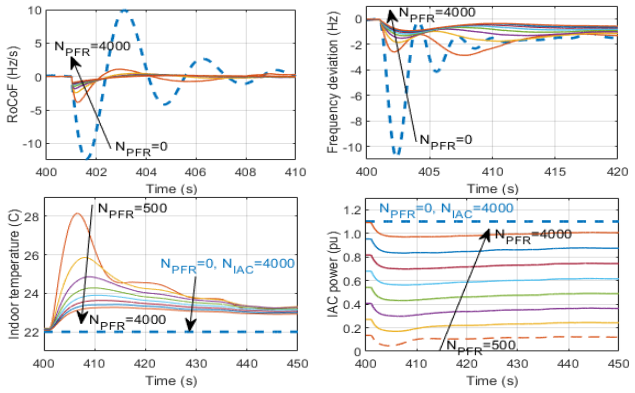

FIGURE 14. Simulation results: Number of IAC for participating in frequency regulations (N_{PFR}) changes.

temperature deviation (bottom of Fig.12) demonstrates that if the indoor temperature weignt w_1 increases, the frequency deviation increases (negative sign), and the indoor temperature deviation decreases. These simulation results were consistent with those shown in Fig. 8 (b). The selection of temperature weight w_1 can be obtained by considering the ability of w_1 to regulate RoCoF, regulate the microgrid frequency, and provide indoor temperatures within acceptable ranges. Temperature weight $w_1 = 1$ can provide lower RoCoF, lower frequency deviation, and indoor temperatures within acceptable ranges. Thus, the temperature weight $w_1 = 1$ was selected as the best temperature weight for utilization in the following subsection.

C. IMPACT OF INERTIA GAIN

The effects of the inertia gain (K_{VI}) on RoCoF, frequency deviation, indoor temperature, and IAC power are shown in Fig. 13. The inertial gain was significant during the contingencies at 400 s. When the inertial gain K_{VI} increases, the first RoCoF oscillation decreases from approximately -1.75 to -0.50. A high K_{VI} provides a higher frequency deviation than a low K_{VI}. In addition, the maximum temperature deviation and maximum IAC consumption power of all K_{VI} are slightly different.

D. IMPACT OF THE NUMBER OF IACs

The impact of the number of inverter air conditioner participating in frequency regulation (N_{PFR}) is shown in Fig. 14. The total number of units is 4000. Thus, $N_{PFR} = 500$ means that the IACs 500 unit is used for frequency regulation, and the IACs 3500 unit ($N_{IAC} = 3500$) is connected to the microgrid as a conventional load. As shown in Fig. 14, when N_{PFR} increased, RoCoF, frequency deviation, and indoor temperature deviation decreased. These simulation results imply that a large number of IACs is better than a small number of IACs. Consequently, in the next subsection, the maximum number of IACs ($N_{PFR} = 4000$) is used.

E. CASE STUDY

The impact of the proposed VESS on the virtual inertia emulators and frequency regulation is explained in this subsection. Participation inverter air conditioners are the main components of the proposed VESS, whereas the photovoltaic generator is an auxiliary component. The photovoltaic generators support the inverter air conditioners when the power consumption of the inverter air conditioners is insufficient in the charging state to support the virtual inertia emulator. Therefore, the charging capacity of the inverter air conditioners (which consume more power than the conventional air conditioner) for a virtual inertia emulator is fulfilled by the charging capacity of the photovoltaic generators (which generates less power than the maximum power point tracking photovoltaic generators).

The efficiency and robustness of the proposed MPC-based VESS from photovoltaic generators and the inverter air conditioner method, called "VESS2." technique was compared with the "NoVESS" and "VESS1." More details are provided below.

"NoVESS" is a microgrid without a virtual energy storage system. Inverter air conditioners consume power as a part of a conventional load. The MPC controls the inverter air conditioners to regulate the indoor temperature.

"VESS1" is a microgrid with the VESS same as the proposed method but the VESS comprises only inverter air conditioners. Photovoltaic generators are not included in virtual inertia emulators or frequency regulations. Consequently, photovoltaic generators operate at maximum power generation.

Case 1: It is assumed that the heat radiation from disturbances increases, that is, $Q_{dis} = 0.55$ (nominal $Q_{dis} = 0.43$). The increase in heat radiation from disturbances resulting from someone opening a door/window and forgetting to close it. Some electrical appliances such as refrigerators can also produce high temperatures. In addition, the outdoor temperature was high at 40 °C. The participating IACs were operated near the maximum power limit to maintain an indoor temperature at a set value of 25 °C. Figure 15 shows the simulation results of Case 1 when the disconnection of wind power plants 0.10 pu. at 200 s and re-connection of wind power plants 0.10 pu. at 500 s (see Fig. 10 for more details of the case study).

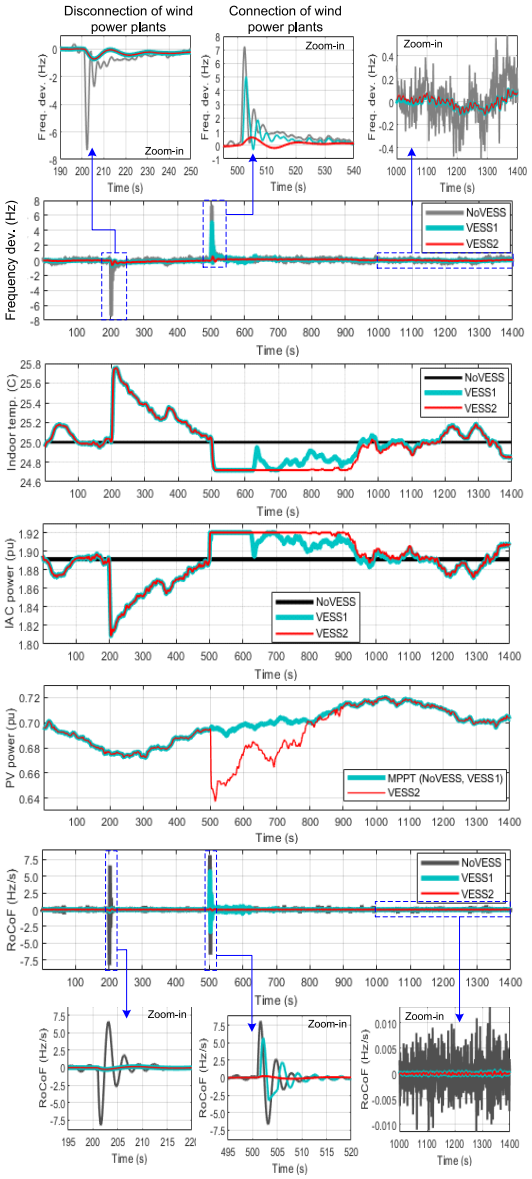

FIGURE 15. Simulation results of Case 1.

At 200 s, the disconnection of the wind power plants 0.10 pu. In this case, NoVESS produces the first RoCoF and a very high-frequency deviation, that is, the first RoCoF $= -7.6$ Hz/s and frequency deviation $= -7.8$ Hz. Conventionally, the operation of the microgrid frequency deviation from the nominal frequency (50 Hz in this study) are in the ranges of ± 1 Hz [34], [35], and the RoCoF are in the ranges of ± 1 Hz/s [36]. This result implies that the NoVESS cannot operate owing to the underfrequency and RoCoF relays tripping [34], [35], [36]. In contrast, VESS1 and VESS2 maintain the virtual inertia and frequency regulation within acceptable limits. The IAC powers of VESS1 and VESS2 can be reduced to support the reduction in the wind power generator.

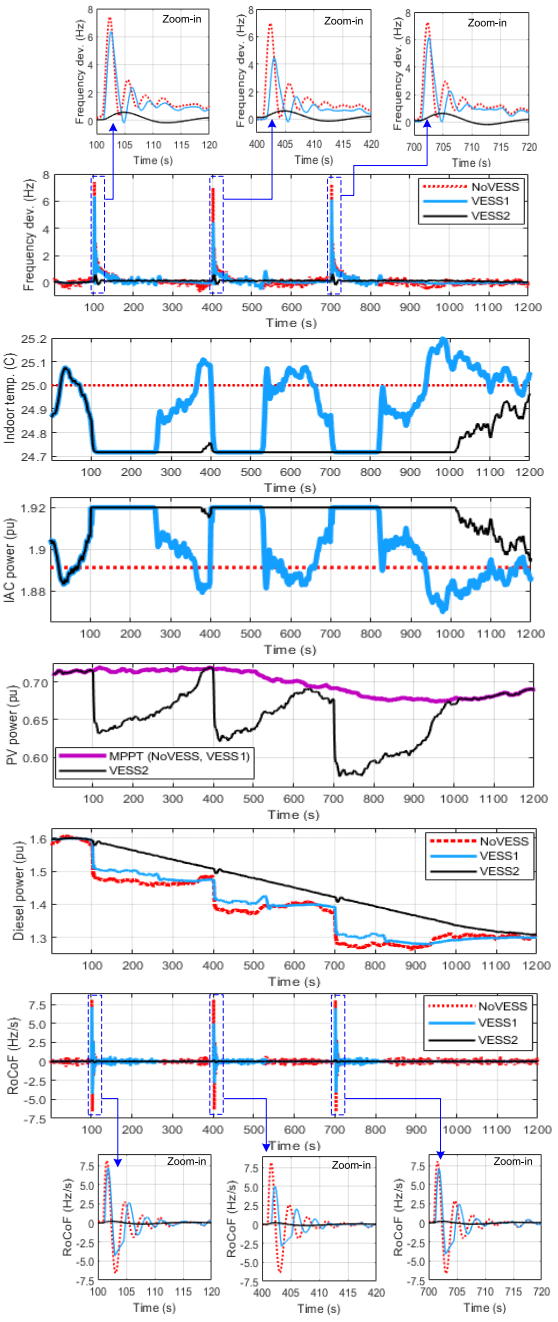

FIGURE 16. Simulation results of Case 2.

The connection of wind power plants 0.10 pu. at 500 s caused a sudden change in the power mismatch between generation and load. NoVESS and VESS1 have very high RoCoFs and frequency deviations. In this case, the IAC power of VESS1 cannot consume power to reduce RoCoF and frequency fluctuations. The output power of the IAC hits the IAC's maximum power limit. Therefore, the frequency deviation over limits (±1 Hz) and RoCoF over limits (±1 Hz/s) cause the operation of over-frequency and RoCoF relays tripping [34], [35], [36], respectively. By contrast, the proposed VESS2 can successfully provide virtual inertia and

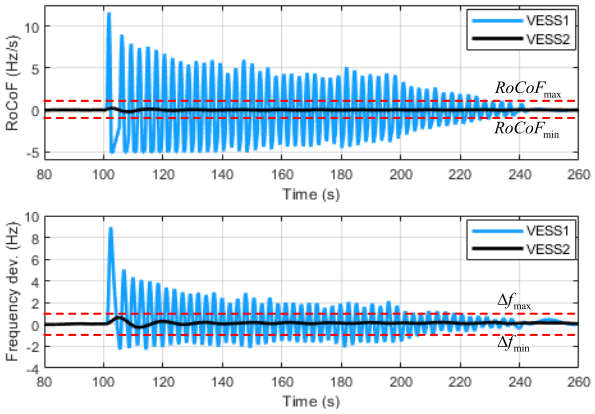

FIGURE 17. Simulation results of Case 3.

frequency regulation. The PV power of VESS2 was used to support the virtual inertia and frequency regulation. The simulation results imply that the proposed VESS2 is better than NoVESS and VESS1 in terms of supporting virtual inertia and frequency regulation when wind-power generation is connected to the microgrid.

Case 2: It is assumed that $Q_{dis} = 0.55$, $T_{ambient} = 40\,^{\circ}C$, and $T_{indoor,set} = 25\,^{\circ}C$ as in Case 1. Figure 16 shows the simulation results of Case 2 when the connection of the wind power plants 0.10 pu. at 100, 400, and 700 s, respectively (see Fig. 10 for further detail). In this case, only VESS2 could successfully provide virtual inertia and frequency regulation. The PV power of VESS2 was used to support the virtual inertia and frequency regulation. The simulation results imply that the proposed VESS2 is better than NoVESS and VESS1 in terms of supporting virtual inertia and frequency regulation when wind-power generation is connected to the microgrid.

Case 3: All situations were assumed to be the same as those in Case 2; however, the inertia constant and damping of the microgrid were changed. Thus, the inertia constant and damping of the microgrid were changed until one of the three methods lacked a frequency stability. Finally, $H = 0.040$ (-33% of the nominal value) and $D = 0.029$ (-76% of the nominal value) causes NoVESSs to lack frequency stability.

Fig. 17 shows the simulation results for Case 3. Note that, in this case, the simulation result of the NoVESS is not shown because of the very high frequency at all times of the simulation. This implies that the NoVESS cannot operate when the microgrid parameters change. As shown in Fig. 17, it can be observed that the proposed VESS2 can successfully reduce the frequency deviation and RoCoF within the acceptable ranges of ±1 Hz and ±1 Hz/s [34], [35], [36], respectively. These results imply that the proposed VESS2 method is robust to variations in microgrid inertia and damping parameters.

VI. CONCLUSION

In this study, a model predictive control (MPC)-based virtual energy storage system (VESS) for virtual inertia control and

frequency regulation was proposed. The VESS comprises photovoltaic (PV) generators and inverter air conditioners (IACs). The VESS controller consists of two loops: (1) an MPC1-based indoor temperature and microgrid frequency control loop and (2) an MPC2-based virtual inertia control loop. The objective of the MPC1 controller is to regulate the indoor temperature and frequency deviation from the reference value. The indoor temperature and frequency deviation signals were weighted appropriately. The objective of the MPC2 is to regulate the rate of change of frequency (RoCoF) by predicting the appropriate inertia gain. The study results are summarized in detail below.

1) The proposed VESS can provide virtual inertia and regulate the frequency of the low inertia microgrid.

2) The proposed VESS has a performance effect over the conventional methods (microgrid without VESS and microgrid with VESS using IACs) when considering the ability to provide virtual inertia and frequency regulation.

3) The proposed MPC-based virtual energy storage system using PV generators and the IACs method can provide virtual inertia and frequency regulation when the microgrid parameters change. The simulation results confirm that the proposed MPC-based virtual energy storage system using PV generators and the IACs method is robust to system parameter variations.

Finally, an MPC-based virtual energy storage system using PV generators and inverter air conditioners for virtual inertia control and microgrid frequency regulation can be regarded as a significant outcome of this study. Eventually, the virtual energy storage system can be used for power system ancillary services. The application of the virtual energy storage system for virtual inertia control and microgrid frequency regulation can be further studied by improving the controller.

REFERENCES

[1] J. Fang, H. Li, Y. Tang, and F. Blaabjerg, "On the inertia of future more-electronics power systems," *IEEE J. Emerg. Sel. Topics Power Electron.*, vol. 7, no. 4, pp. 2130–2146, Dec. 2019.

[2] J. Fang, H. Li, Y. Tang, and F. Blaabjerg, "Distributed power system virtual inertia implemented by grid-connected power converters," *IEEE Trans. Power Electron.*, vol. 33, no. 10, pp. 8488–8499, Oct. 2018.

[3] T. Kerdphol, F. S. Rahman, M. Watanabe, Y. Mitani, D. Turschner, and H. P. Beck, "Enhanced virtual inertia control based on derivative technique to emulate simultaneous inertia and damping properties for microgrid frequency regulation," *IEEE Access*, vol. 7, pp. 14422–14433, 2019.

[4] U. Akram, N. Mithulananthan, M. Q. Raza, R. Shah, and F. Milano, "RoCoF restrictive planning framework and wind speed forecast informed operation strategy of energy storage system," *IEEE Trans. Power Syst.*, vol. 36, no. 1, pp. 224–234, Jan. 2021.

[5] R. Yan, N.-A.-Masood, T. K. Saha, F. Bai, and H. Gu, "The anatomy of the 2016 South Australia blackout: A catastrophic event in a high renewable network," *IEEE Trans. Power Syst.*, vol. 33, no. 5, pp. 5374–5388, Sep. 2018.

[6] A. Pandey, S. Kumar, S. Mohire, P. Pentayya, and F. Kazi, "Dynamic modeling and cascade failure analysis of the Mumbai grid incident of October 12, 2020," *IEEE Access*, vol. 10, pp. 43598–43610, 2022.

[7] M. Cheng, S. S. Sami, and J. Wu, "Benefits of using virtual energy storage system for power system frequency response," *Appl. Energy*, vol. 194, pp. 376–385, May 2017.

[8] H. Saberi, C. Zhang, and Z. Y. Dong, "Capacity of virtual energy storage system for frequency regulation services via a data-driven distributionally robust optimization method," *IEEE Trans. Power Syst.*, early access, Jul. 29, 2022, doi: 10.1109/TPWRS.2022.3193899.

[9] T. Ding, X. Zhang, R. Lu, M. Qu, M. Shahidehpour, Y. He, and T. Chen, "Multi-stage distributionally robust stochastic dual dynamic programming to multi-period economic dispatch with virtual energy storage," *IEEE Trans. Sustain. Energy*, vol. 13, no. 1, pp. 146–158, Jan. 2022.

[10] S. Kumar, V. Krishnasamy, R. Kaur, and N. K. Kandasamy, "Virtual energy storage-based energy management algorithm for optimally sized DC nanogrid," *IEEE Syst. J.*, vol. 16, no. 1, pp. 231–239, Mar. 2022.

[11] A. Niromandfama, A. M. Pour, and E. Zarezadehd, "Virtual energy storage modeling based on electricity customers' behavior to maximize wind profit," *J. Ener. Storage*, vol. 32, pp. 1–13, Dec. 2020.

[12] K. Vijayalakshmi, K. Vijayakumar, and K. Nandhakumar, "Prediction of virtual energy storage capacity of the air-conditioner using a stochastic gradient descent based artificial neural network," *Elec. Pow. Syst. Res.*, vol. 208, pp. 1–10, Jul. 2022.

[13] D. Chakravorty, B. Chaudhuri, and S. Y. R. Hui, "Rapid frequency response from smart loads in great Britain power system," *IEEE Trans. Smart Grid*, vol. 8, no. 5, pp. 2160–2169, Sep. 2017.

[14] M. Malekpour, R. Azizipanah-Abarghooee, F. Teng, G. Strbac, and V. Terzija, "Fast frequency response from smart induction motor variable speed drives," *IEEE Trans. Power Syst.*, vol. 35, no. 2, pp. 997–1008, Mar. 2020.

[15] D. Terazono, J. Liu, Y. Miura, S. Sakabe, H. Bevrani, and T. Ise, "Grid frequency regulation support from back-to-back motor drive system with virtual-synchronous-generator-based coordinated control," *IEEE Trans. Power Electron.*, vol. 36, no. 3, pp. 2901–2913, Mar. 2021.

[16] T. Chen, J. Guo, B. Chaudhuri, and S. Y. Hui, "Virtual inertia from smart loads," *IEEE Trans. Smart Grid*, vol. 11, no. 5, pp. 4311–4320, Sep. 2020.

[17] H. Hui, Y. Ding, and M. Zheng, "Equivalent modeling of inverter air conditioners for providing frequency regulation service," *IEEE Trans. Ind. Electron.*, vol. 66, no. 2, pp. 1413–1423, Feb. 2019.

[18] T. Jiang, P. Ju, C. Wang, H. Li, and J. Liu, "Coordinated control of air-conditioning loads for system frequency regulation," *IEEE Trans. Smart Grid*, vol. 12, no. 1, pp. 548–560, Jan. 2021.

[19] N. Zhao, S. Gorbachev, D. Yue, V. Kuzin, C. Dou, X. Zhou, and J. Dai, "Model predictive based frequency control of power system incorporating air-conditioning loads with communication delay," *Int. J. Elect. Pow. Ener. Syst.*, vol. 138, pp. 1–8, Jun. 2022.

[20] J. Pahasa, P. Potejana, and I. Ngamroo, "Multi-objective decentralized model predictive control for inverter air conditioner control of indoor temperature and frequency stabilization in microgrid," *Energies*, vol. 14, no. 21, pp. 1–28, Oct. 2021.

[21] D. Zhang, C. Li, S. Luo, D. Luo, M. Shahidehpour, C. Chen, and B. Zhou, "Multi-objective control of residential HVAC loads for balancing the User's comfort with the frequency regulation performance," *IEEE Trans. Smart Grid*, vol. 13, no. 5, pp. 3546–3557, Sep. 2022.

[22] X. Ge, X. Zhu, Y. Fu, Y. Xu, and L. Huang, "Optimization of reserve with different time scales for wind-thermal power optimal scheduling considering dynamic deloading of wind turbines," *IEEE Trans. Sustain. Energy*, vol. 13, no. 4, pp. 2041–2050, Oct. 2022.

[23] B. Liu, J. Zhao, Q. Huang, F. Milano, Y. Zhang, and W. Hu, "Nonlinear virtual inertia control of WTGs for enhancing primary frequency response and suppressing drivetrain torsional oscillations," *IEEE Trans. Power Syst.*, vol. 36, no. 5, pp. 4102–4113, Sep. 2021.

[24] P. Saxena, N. Singh, and A. K. Pandey, "Self-regulated solar PV systems: Replacing battery via virtual inertia reserve," *IEEE Trans. Energy Convers.*, vol. 36, no. 3, pp. 2185–2194, Sep. 2021.

[25] Q. Peng, Z. Tang, Y. Yang, T. Liu, and F. Blaabjerg, "Event-triggering virtual inertia control of PV systems with power reserve," *IEEE Trans. Ind. Appl.*, vol. 57, no. 4, pp. 4059–4070, Jul. 2021.

[26] J. Chang, Y. Du, E. Lim, H. Wen, X. Li, and J. Lin, "Coordinated frequency regulation using solar forecasting based virtual inertia control for islanded microgrids," *IEEE Trans. Sustain. Energy*, vol. 12, no. 4, pp. 2393–2403, Oct. 2021.

[27] Q. Peng, Y. Yang, T. Liu, and F. Blaabjerg, "Coordination of virtual inertia control and frequency damping in PV systems for optimal frequency support," *CPSS Trans. Power Electron. Appl.*, vol. 5, no. 4, pp. 305–316, Dec. 2020.

[28] A. Khazali, N. Rezaei, H. Saboori, and J. Guerrero, "Using PV systems and parking lots to provide virtual inertia and frequency regulation provision in low inertia grids," *Elect. Pow. Syst. Res.*, vol. 207, pp. 1–15, Jun. 2022.

[29] J. Pahasa and I. Ngamroo, "Coordinated PHEV, PV, and ESS for microgrid frequency regulation using centralized model predictive control considering variation of PHEV number," *IEEE Access*, vol. 6, pp. 69151–69161, 2018.
[30] A. Fawzy, A. Bakeer, G. Magdy, I. E. Atawi, and M. Roshdy, "Adaptive virtual inertia-damping system based on model predictive control for low-inertia microgrids," *IEEE Access*, vol. 9, pp. 109718–109731, 2021.
[31] N. Mahdavi, J. H. Braslavsky, M. M. Seron, and S. R. West, "Model predictive control of distributed air-conditioning loads to compensate fluctuations in solar power," *IEEE Trans. Smart Grid*, vol. 8, no. 6, pp. 3055–3065, Nov. 2017.
[32] A. Bemporad, N. L. Ricker, and M. Morari, "*Model Predictive Control Toolbox User's Guide*. Natick, MA, USA: The MathWorks, 2010.
[33] W. Chen, J. Qiu, J. Zhao, Q. Chai, and Z. Y. Dong, "Bargaining game-based profit allocation of virtual power plant in frequency regulation market considering battery cycle life," *IEEE Trans. Smart Grid*, vol. 12, no. 4, pp. 2913–2928, Jul. 2021.
[34] *IEEE Guide for Design, Operation, and Integration of Distributed Resource Island Systems With Electric Power Systems*, IEEE Standard 1547.4–2011, Jul. 2011, pp. 1–54.
[35] A. Mondal and M. S. Illindala, "Improved frequency regulation in an islanded mixed source microgrid through coordinated operation of DERs and smart loads," *IEEE Trans. Ind. Appl.*, vol. 54, no. 1, pp. 112–120, Jan. 2018.
[36] M. Grebla, J. R. A. K. Yellajosula, and H. K. Hoidalen, "Adaptive frequency estimation method for ROCOF islanding detection relay," *IEEE Trans. Power Del.*, vol. 35, no. 4, pp. 1867–1875, Aug. 2020.
[37] J. M. S. De Araujo, "WRF wind speed simulation and SAM wind energy estimation: A case study in Dili Timor Leste," *IEEE Access*, vol. 7, pp. 35382–35393, 2019.

JONGLAK PAHASA (Member, IEEE) received the B.Eng. degree in electrical engineering from the King Mongkut's Institute of Technology Ladkrabang (KMITL), Bangkok, Thailand, in 1997, the M.Eng. degree in electrical engineering from Chiang Mai University, Chiang Mai, Thailand, in 2007, and the D.Eng. degree in electrical engineering from KMITL, in 2011.

She is currently an Associate Professor at the School of Engineering, University of Phayao, Phayao, Thailand. Her current research interests include the applications of artificial intelligence in power system stability and control.

POTEJANASAK POTEJANA was born in Phrae, Thailand, in 1982. He received the B.Eng. degree in production engineering from the King Mongkut's University of Technology North Bangkok (KMUTNB), Bangkok, in 2004, the M.Eng. degree in industrial engineering from Kasetsart University, Bangkok, in 2009, and the D.Eng. degree in mechanical and control engineering from the Tokyo Institute of Technology, Tokyo, Japan, in 2016.

He is currently an Assistant Professor at the School of Engineering, University of Phayao, Thailand. His research interests include nanofabrication methods for micro- or nanostructured surfaces and nanophotonic devices.

ISSARACHAI NGAMROO (Senior Member, IEEE) received the Ph.D. degree in electrical engineering from Osaka University, Osaka, Japan, in 2000.

He is currently a Professor at the School of Engineering, King Mongkut's Institute of Technology Ladkrabang (KMITL), Bangkok, Thailand. His research interests include power-system stability, dynamics, and control.